Products and Mechanisms of Ozone Reactions with Oleic Acid for Aerosol Particles Having Core−Shell Morphologies

Yasmine Katrib,[†] Scot T. Martin,*[,†] Hui-Ming Hung,[†] Yinon Rudich,[‡] Haizheng Zhang,[§] Jay G. Slowik,[§] Paul Davidovits,[§] John T. Jayne,[⊥] and Douglas R. Worsnop[⊥]

Division of Engineering and Applied Sciences, 29 Oxford St., Pierce Hall, Room 122, Harvard University, Cambridge, Massachusetts 02138, Department of Environmental Sciences, Weizmann Institute, Rehovot 76100, Israel, Chemistry Department, Boston College, Chestnut Hill, Massachusetts 02467, and Aerodyne Research, Inc., 45 Manning Road, Billerica, Massachusetts 08121-3976

Received: January 16, 2004; In Final Form: April 28, 2004

Heterogeneous reactions of oleic acid aerosol particles with ozone are studied below 1% relative humidity. The particles have inert polystyrene latex cores (101-nm diameter) coated by oleic acid layers of 2 to 30 nm. The chemical content of the organic layer is monitored with increasing ozone exposure by using an aerosol mass spectrometer. The carbon-normalized percent yields of particle-phase reaction products are 20−35% 9-oxononanoic acid, 1−3% azelaic acid, 1−3% nonanoic acid, and 35−50% other organic molecules (designated as CHO_T). There is approximately 25% evaporation, presumably as 1-nonanal. To explain the formation of CHO_T molecules and the low yields of azelaic and nonanoic acids, we suggest a chemical mechanism in which the Criegee biradical precursors to azelaic acid and nonanoic acid are scavenged by oleic acid to form CHO_T molecules. These chemical reactions increase the carbon-normalized oxygen content (z/x) of the $C_xH_yO_z$ layer from 0.1 for unreacted oleic acid to 0.25 after high ozone exposure. Under the assumption that oxygen content is a predictor of hygroscopicity, our results suggest an increased cloud condensation nuclei activity of atmospherically aged organic particles that initially have alkene functionalities.

1. Introduction

Atmospheric particles affect the environment in many ways. On the global scale, they directly and indirectly affect radiative forcing and the hydrological cycle.[1−5] On the regional scale, they have a primary role in air pollution, visibility, and human health.[6] Quantifying these roles is challenging, in part because atmospheric particles have a complex structure and chemical composition. For example, organic coatings can form on inorganic particles such as sea salt and dust.[7−12] In some cases, these organic coatings control particle hygroscopicity and heterogeneous chemical reactivity.[13,14] Widespread occurrence of organic and inorganic species, which are also often mutually and homogeneously mixed within the same particle,[15−17] implies a broad impact for the organic chemical fraction of atmospheric particles.[18−26]

Heterogeneous oxidation reactions are an important process in the aging of the organic fraction in atmospheric particles, specifically in affecting their chemical composition and hygroscopic properties. A key unknown is an understanding of the chemical reactions between the organic particulate matter and atmospheric oxidants such as O_3, NO_3, and OH.[27−34] Condensed-phase organic molecules typically react much faster than their gas-phase counterparts: 1 in 10^3 collisions between O_3 molecules and liquid oleic acid molecules leads to chemical reaction, which compares to 1 in 10^6 in the gas phase.[30,35,36] However, the products formed are uncertain, although they generally contain additional oxygen atoms.

The formation of oxygenated products during atmospheric residence leads to a general increase in the carbon-normalized oxygen content (z/x) of the average chemical composition $C_xH_yO_z$ of the particle. An associated increase in particle hygroscopicity and cloud condensation nuclei (CCN) effectiveness is expected.[13,37] With the current state of knowledge, however, many assumptions are required for the formulation of kinetic models and of reaction mechanisms relevant to the aging of particles and the conversion from hydrophobic to hydrophilic properties. A need exists to understand and quantify the chemical aging processes of organic particles.

As a model system for complex multicomponent atmospheric particles, in this paper we examine the ozone reaction with particles having a surface layer of varying thickness of oleic acid ($C_{18}H_{34}O_2$). Particle oleic acid concentrations are approximately 1 ng m^{-3} in urban aerosol.[38] The double bond of oleic acid is susceptible to attack by ozone, which is believed to lead to the formation of a primary ozonide (molozonide) (Figure 1).

The molozonide decomposes when a pair of O−O and C−C bonds break, which allows for two alternative reaction pathways. Azelaic acid (AA) and 1-nonanal (NN) are believed to form in pathway 1, while pathway 2 is expected to yield 9-oxononanoic acid (OA) and nonanoic acid (NA). NN has a higher vapor pressure and is expected to volatilize. Although AA, OA, and NA have low vapor pressures and are surmised to remain in the particle, a summary of previous work (Table 1) shows that a thorough analysis of the possible particle-phase products has not been undertaken (i.e., the numerous "n/a" designations). Furthermore, there is an absence of quantitative particle-phase

* Author to whom correspondence should be addressed. E-mail: scot_martin@harvard.edu. Web: http://www.deas.harvard.edu/~smartin.
[†] Harvard University.
[‡] Weizmann Institute.
[§] Boston College.
[⊥] Aerodyne Research, Inc.

10.1021/jp049759d CCC: $27.50
Published on Web 07/16/2004

TABLE 1: Comparison of Techniques, Oleic Acid Layer Thickness, Ozone Exposure, Water Partial Pressure, Phase Analyzed (i.e., particle versus gas), and Products Identified for Oleic Acid Reactions with Ozone[a]

	technique	oleic acid thickness	ozone exposure (atm·s)	P_{H_2O} (Torr)	phase studied	identified products
this work aerosol study	AMS	2−30 nm	1×10^{-5}	0.2	condensed	OA (major) AA (minor) NA (minor) NN (not present) other $C_xH_yO_z$ products (major)
Morris et al.[29] aerosol study	AMS	200−600 nm	1×10^{-5}	−	condensed	OA (n/a) AA (n/a) NA (n/a) NN (n/a)
Smith et al.[33] aerosol study	SMS	>1 μm	8×10^{-4}	−	condensed	OA (identified) AA (n/a) NA (n/a) NN (n/a)
Moise and Rudich[39] coated wall flow tube study	GMS, IC	millimeters	10^{-7}	−	condensed and gas	OA (n/a) AA (identified, off-line) NA (n/a) NN (gas, 25% yield)
Thornberry and Abbatt[30] coated wall flow tube study	GMS	millimeters	10^{-7}	−	gas	NN (gas, 25% yield)

[a] The designation "n/a" indicates that the analysis method is not performed for these chemical species. Key: AMS, aerosol mass spectrometer; SMS, single-particle mass spectrometer; GMS, gas-phase mass spectrometry; and IC, ion chromatography of condensed-phase products. (1 atm of O_3 is 2.46×10^{19} molecules cm^{-3}.)

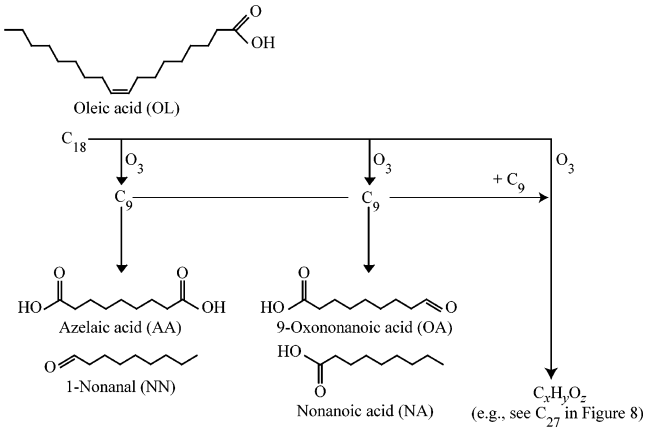

Figure 1. Reaction pathways of oleic acid with ozone. Shown are pathways to form AA and NA by carboxylate formation on the right side of the double bond and to form OA and NA by carboxylate formation on the left side of the double bond. Also shown is a third pathway hypothesized by the results of the current work, which involves the reaction of ozone, oleic acid, and a C_9 product to form $C_xH_yO_z$ products (see text). Key: AA, azelaic acid; NN, 1-nonanal; OA, 9-oxononanoic acid; NA, nonanoic acid.

product yields in all previous studies. An important aspect of our current work is the capability to directly identify and quantify the condensed-phase products of the in situ aerosol.

We determine the chemical composition of the particles and the product yields after ozone exposure by using an Aerodyne aerosol mass spectrometer (AMS). In addition to pathways 1 and 2 (Figure 1), we find that other organic molecules form, indicating complex reaction pathways possibly mediated by Criegee biradicals.[29,33,39] Another important aspect of the current study is that we probe the formation of products in the particles as a function of the layer thickness from 2 to 30 nm. To carry out this work, we develop a vaporization-condensation method for generating an inert polystyrene latex particle core (101-nm diameter) coated with oleic acid layers of variable thickness (2 to 30 nm). An important conclusion from previous studies is that the diffuso-reactive length of O_3 in oleic acid is approximately 10 nm.[29,33,39] Our hypothesis is that a dependence of product yield on oleic acid layer thickness can identify the reaction pathways that occur mostly in the surface region.

2. Experimental Section

An overview of the experimental setup and protocol is as follows. Nonvolatile core particles of polystyrene latex (PSL) are generated by using an atomizer. Following a drying stage that decreases relative humidity below 1%, the particles are coated with oleic acid by passing through a heated tube having a linear hot-to-cool temperature gradient along its length. The layer thickness of oleic acid is variable and is adjusted by controlling the concentration of the oleic acid at the entry of the heated tube. The coated particles are then exposed to variable ozone concentrations. The loss of parent oleic acid and the appearance of chemical products in the organic layer are quantified with an Aerodyne aerosol mass spectrometer (AMS).

2.1. Generation of Coated Particles. Oleic acid particles, formed by vapor condensation over a heated oleic acid liquid reservoir (50 to 70 °C), are transported at 0.1 Lpm and externally mixed downstream with nonvolatile core particles (Figure 2). These core particles are 101 nm polystyrene latex (PSL) (Duke Scientific), which are atomized into an aerosol flow (1 Lpm). The combined externally mixed aerosol passes through a tube furnace having a linear hot-to-cool temperature gradient (78 to 25 °C): the oleic acid particles vaporize in the hot region, and the vapor subsequently condenses in the cool region onto the surfaces of the PSL particles.[40] Internally mixed coated particles result. The temperature of the reservoir, the gradient of the oven, and the adjustable flow are the levers controlling the layer thickness of oleic acid. Using this apparatus, 101 nm PSL particles coated with oleic acid layers varying from 2 to 30 nm are generated in a reproducible and controlled manner in number concentrations of 10^3 particles cm^{-3}. (In the experiments for thicker layer thickness, a second mode near 60-nm diameter is also observed, presumably arising from homogeneous nucleation of oleic acid. The relative contribution to total aerosol oleic acid mass, however, is approximately 5%. This homogeneous mode is omitted in our data analysis.)

A scanning mobility particle sizer (SMPS) with isokinetic sampling is employed to measure the number size distribution

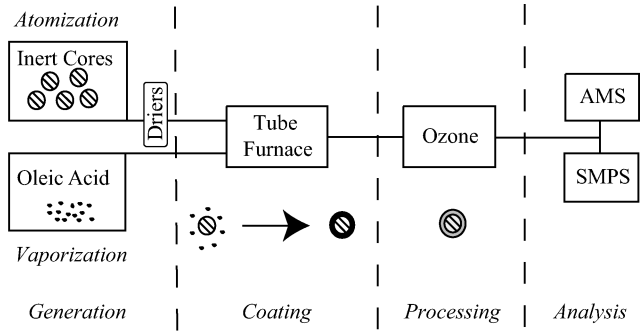

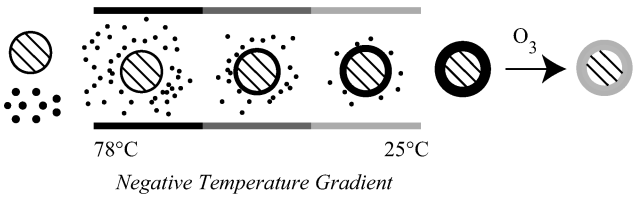

Figure 2. Top: Experimental apparatus for particle generation, coating, processing, and analysis. Bottom: Coating process inside the tube furnace followed by reaction with ozone. Key: AMS, aerosol mass spectrometer; SMPS, scanning mobility particle sizer.

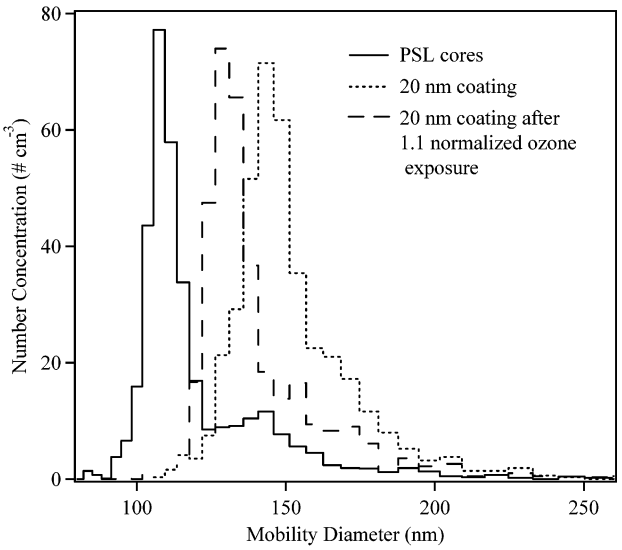

Figure 3. SMPS number size distribution measurements of uncoated polystyrene (PSL) particles, particles coated by oleic acid (20 nm), and particles coated by oleic acid and products after 1.1 normalized ozone exposure. The original layer thickness of 20 nm decreases to 15 nm following ozone exposure.

of coated PSL particles. At low PSL concentrations, the distribution is symmetric and is limited by the DMA transfer function.[35] Examples of uncoated PSL particles and PSL particles having a 20 nm oleic acid coating are shown in Figure 3. The increase of the particle mobility diameter beyond that of the PSL core (101 nm) is twice the oleic acid layer thickness, assuming a uniform coating on spherical particles. The original layer thickness of 20 nm decreases to 15 nm following ozone exposure (Figure 3).

At the high PSL concentrations necessary for sufficient mass loading in the AMS analysis, PSL coagulation occurs in some of our experiments. Larger particles apparent in these distributions arise from a combination of factors, including coagulation of PSL particles prior to atomization (i.e., in the aqueous PSL suspension in the reservoir) and dried nonvolatile inorganic impurities initially present in the water. An example of coagulation is apparent in the second mode centered at 143 nm for the PSL particles (Figure 3).

Complementary to the mobility diameter measured by the SMPS, the AMS measures the particle aerodynamic diameter. Whereas the mobility diameter decreases (Figure 3), the aerodynamic diameter increases (not shown) after reaction with ozone. Morris et al.[29] and Smith et al.[33] report that aerodynamic diameter increases upon ozone exposure, whereas Broekhuizen et al.[41] report a decrease in mobility diameter similar to our observations. For spherical particles, a decrease in mobility diameter coupled to an increase in aerodynamic diameter implies that particle mass density increases. Oxygenated products of oleic acid are expected to increase density. A fuller report on this topic is forthcoming from us.

2.2. Chemical Composition of the Organic Layer. The mass loading of particle-phase oleic acid and its oxidation products is obtained with use of an aerosol mass spectrometer (AMS).[42] The AMS is composed of three main sections: (1) particle sampling into high vacuum (10^{-5} Torr) through a critical orifice, (2) aerodynamic sizing via particle time-of-flight (TOF) measurement, and (3) particle analysis with mass spectrometry (MS).

For the MS analysis, the particle beam is directed onto a resistively heated hotplate (ca. 350 °C), where the volatile and semivolatile constituents of the particle flash vaporize upon impact. The volatilized molecules are ionized by electron impact at 70 eV, and the positive ions of the fragments pass through a quadrupole mass filter and are detected as a current at the electron multiplier. The detection process has sufficient mass sensitivity and time response to detect single particle vaporization events for a fixed *m*/*z* value. The AMS, therefore, provides primary measurements of particle number size distribution (number of particles cm^{-3}·air/d log D_p) and mass loading at a specific *m*/*z* value (μg m^{-3}/d log D_p) for any particle yielding a positive ion fragment at the tuned *m*/*z* value. (The connection between the electron multiplier current and the mass loading is discussed in section 2.4.) Given an aerosol input of constant composition, as is true for our laboratory studies, the *m*/*z* value can be scanned to provide size-resolved mass spectra of the particle ensemble. For our experimental conditions (10^3 particle cm^{-3}, 0.1 Lpm sampling, 75% transmission efficiency, and 300 ms *m*/*z* dwell time), each mass loading at specific *m*/*z* value is an average of approximately 300 individual particles.

In the current paper, MS results are integrated across the aerosol size distribution, and the size-resolved capability is not fully exploited. (The measurement of the particle aerodynamic diameter is employed to determine that the density of a reacted particle increases.) The analytical capability of the AMS is employed to measure the loss of oleic acid and the appearance of oxidation products occurring with ozone exposure. Although the SMPS measurements show 2-, 4-, 6-, and 8-nm coatings, only the 8 nm and thicker coatings have sufficient mass for detection by the AMS when operated in its size-resolving mode. For thinner coatings, we leave open the AMS chopper for 100% duty cycle. With this approach, we obtain the mass spectrum without a particle sizing capability.

2.3. Ozone Flow Tubes Studies. Ozone reaction with oleic acid is studied by coupling an aerosol flow reactor ($^1/_2$ in. i.d., 85 cm length) to the SMPS/AMS system. At the exit of the tube furnace (Figure 2), the coated particles are exposed to ozone, which is produced by a 254-nm UV source and oxygen using a Jelight Model 600 ozone generator. The ozone exposure

TABLE 2: Selected Values of the Normalized Fragmentation Pattern (f_i^j) Measured with the AMS, Where *i* is the *m*/*z* Value and *j* is a Specific Chemical Species (e.g., oleic acid)[a]

m/*z*	OL	OA	AA	NA	NN[b]	CHO_T
44	0.006	0.035	0.008	0.002	0.072	0.02
142	0.0002				0.001	0.0008
144	0.0002	0.0003				0.002
152	0.002		0.025			
155	0.0009	0.002				0.03
158	0.0001			0.001		0.0004
221	0.001					0.002
265	0.001					0.001
282	0.0004					
RIE	1.4	1.4	1.4	1.4	1.4	1.4
MW	282	172	188	158	142	see text
n	18	9	9	9	9	see text

[a] See further discussion in text. Also given are relative ionization efficiency (RIE) compared to nitrate, molecular weight (MW), and number of carbon atoms (*n*). Key: OL, oleic acid; OA, 9-oxononanoic acid; AA, azelaic acid; NA, nonanoic acid; NN, 1-nonanal; and the products CHO_T. [b] NIST gas-phase fragmentation pattern given for NN (see text).

(atm.sec) is adjusted by varying the ozone concentration from 1 to 30 ppmV while the interaction time is constant at 3 s. Reaction conditions are 298 K, 1 atm of N_2, and under 1% relative humidity. Ozone concentration is measured by light extinction at 254 nm, using a Hg line lamp and a photodiode detector along a 1-cm path. An absorption cross-section of 1.15×10^{-17} cm^2 molecule^{-1} is employed. Ozone is injected at a variable concentration, and the changes in particle reaction products are determined by AMS analysis.

2.4. Analysis Methods for Quantification of the Products. Ozone reactions modify the particle-phase chemical composition and hence the aerosol mass spectrum. To identify and quantify the molecules present, we deconvolute the mass spectrum using the principles of linear analysis, as explained in detail below.

The electron multiplier current of the AMS at each *m*/*z* value is a direct measure of the number of ions. The two key operative physical principles for mass determination are (1) that the number of ions generated by electron impact through a thin path is proportional to the number of electrons in a bolus of a material (i.e., a particle) and (2) that the number of electrons is proportional to the mass of the bolus. The first proportionality constant is the ionization cross section, while the second is determined by the approximate 1 electron to 1 proton to 1 neutron relationship among light elements. On the basis of these principles, the AMS software employs the ionization efficiency (IE) of nitrate, which is obtained in a daily calibration procedure with a test ammonium nitrate aerosol having a measured mass of nitrate, to convert the current at the electron multiplier into the nitrate equivalent mass (m_i, μg·NO_3 m^{-3}) at each *m*/*z* value (*i*). (For this approach to be accurate, the *m*/*z* values of all ions generated from the bolus of material must be scanned.) The m_i values are shown as the *y*-axes of Figures 4, 5, and 7. They must be corrected by the ionization efficiency of each organic molecule relative to nitrate (RIE^j, no units) (Table 2) to obtain the organic molecule mass loadings (m_i^j, μg·organic m^{-3}), where *j* is a specific chemical species (viz. $j \in$ OL, OA, AA, NA, NN, and CHO_T). The RIE^j values OL, OA, AA, and NA are determined from pure compounds.[42] (Products CHO_T are discussed in detail later.) The recorded mass at each *m*/*z* value is given by $m_i = \sum_j (m_i^j/RIE^j)$.

Each organic molecule has a specific fragmentation pattern f_i^j (μg·organic m^{-3}), normalized such that $1 = \sum_i f_i^j$. We have $m_i^j = \alpha^j f_i^j$, where α^j is a must-be-determined scaling factor and depends on the amount of the organic molecule present. We obtain the α^j values by a linear combination analysis of the recorded spectrum, using the fragmentation patterns as the basis set. The governing *i* equations requiring simultaneous solution are as follows:

$$m_i = \sum_j \frac{\alpha^j f_i^j}{\mathrm{RIE}^j} \tag{1}$$

In matrix form, $[m] = [f][\beta]$, where $[m]$ is a column matrix of *i* rows, $[f]$ is the fragmentation pattern matrix of *i* rows and *j* columns, and $[\beta]$ is the column matrix of unknown chemical mass loadings having *j* rows (i.e., *j* products). Elements of $[\beta]$ are $\beta^j = \alpha^j/\mathrm{RIE}^j$. Once the system of equations is solved for the α^j values, the total mass loading of each product (C^j, μg m^{-3}) is given by $C^j = \sum_i m_i^j = \sum_i \alpha^j f_i^j$.

The percent yield (Y^j) of each condensed-phase product relative to the initial oleic acid concentration is determined on a carbon number basis, as follows:

$$Y^j = 100 \frac{n^j/\mathrm{M_W}^j}{n^{OL}/M_W^{OL}} \frac{C^j}{C_0^{OL}} \tag{2}$$

where n^j is the number of carbon atoms in the molecule *j*, $\mathrm{M_W}^j$ is the molecular weight of molecule *j* (see Table 2), and C_0^{OL} is the oleic acid mass loading at zero ozone exposure. The percent evaporation (Y_E) of the particle is given as $Y_E = 100 - \sum_j Y^j$.

3. Results and Discussion

3.1. Control Experiments. The following control experiments set the framework for the interpretation of our data. No organic material is detected by the AMS for PSL particles alone; PSL particles $(C_8H_8)_n$ do not vaporize until an AMS heater temperature of 850 °C, which is 500 °C above our normal operating conditions. Similarly, no organic material is detected when PSL particles alone are exposed to ozone. When oleic acid is included in the experiments, only its mass spectrum is observed until ozone is added. The oleic acid fragmentation patterns obtained for pure OL particles versus OL-coated PSL particles are the same, from which we conclude that the morphology of the studied particles does not affect the mass spectra. For particles coated by oleic acid and reacted with ozone, the total organic mass detected is independent of the heater temperature for 150 to 600 °C, which indicates that we quantitatively vaporize all semivolatile organics in the reacted outer layer of the particles. Another possible complication ruled out is that reacted organic material could over time condense on the inner walls of the tube furnace when cooled. When next heated, these products could volatilize and complicate our product analysis. However, heating the tube furnace after several weeks of experiments shows neither organic material in the AMS nor particles in the SMPS, both in the presence and absence of ozone.

3.2. Aerosol Mass Spectrometry of Authentic Standards. The sources of our authentic standards are as follows: OL (CAS 112-80-1, NIST MS No. 228066, above 99% purity, Aldrich), AA (CAS 123-99-9, NIST MS No. 113078, 99% purity, Aldrich), OA (NIST MS No. 144254, 98%, Larodan), NA (CAS 112-05-0, NIST MS No. 227949, 98% purity, Aldrich), and NN (CAS 124-19-6, NIST MS No. 232162, 98% purity, Aldrich). The particle-phase MS fragmentation patterns (Figure 4) of the authentic standards of OL, AA, OA, and NA compare well with

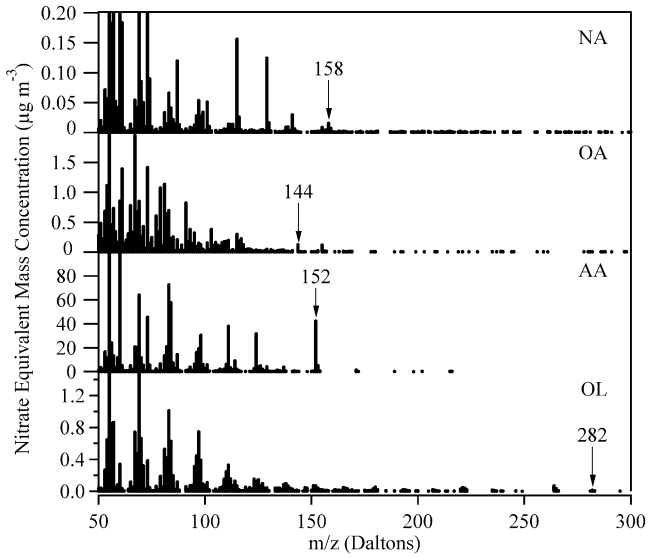

Figure 4. Reference mass spectra for OL, AA, OA, and NA. The principal peaks for the chemical species are 282 amu for OL, 152 amu for AA, 144 amu for OA, and 158 amu for NA. See also Table 2.

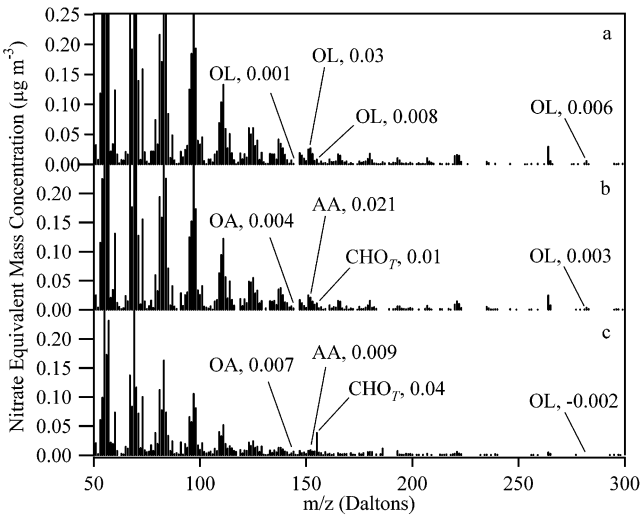

Figure 5. (a) Mass spectrum of pure oleic acid particles. (b) Mass spectrum after ozone exposure of 1.98×10^{-5} atm·s. (c) Mass spectrum after ozone exposure of 6.6×10^{-5} atm·s. Identified peaks are 152 amu for AA, 144 amu for OA, 155 amu for CHO_T, and 282 amu for OL. The numbers next to each label are the *y*-axis values at the specific *m*/*z* value. Conditions: 11 nm coating on PSL core.

the gas-phase MS patterns of the national institute and technology issues (NIST) library (not shown), although there is some variation in the relative intensities of the peaks, which could be explained by differing ionization settings and mass filters (i.e., quadrupole versus magnetic sector) of the AMS and the NIST procedures.[43] Table 2 summarizes the observed fragmentation patterns at important *m*/*z* values. The relative intensities of fragmentation patterns in the AMS analysis are reproducible within 5%.

Aerosol is obtained for AMS analysis by atomizing the authentic standards individually in methanol; whether atomized or obtained by vapor condensation, the OL mass spectrum is similar. NN also prepared in methanol does not yield an aerosol mass spectrum, presumably due to its high volatility. The NIST database provides the gas-phase NN fragmentation pattern. On the basis of this fragmentation pattern, NN is never detected by us when oleic acid is exposed to ozone, viz. $\alpha^{NN} = 0$.

3.3. Reaction Pathways upon Ozone Exposure. In the following sections, we discuss the formation of OA, AA, NA, and CHO_T products (section *3.3.1* and section *3.3.2*), the effects of layer thickness on those products (section *3.3.3*), and the increase in chemical oxygen content with increasing ozone exposure (section *3.3.4*).

3.3.1. OA, AA, and NA Products. An example of raw data demonstrating the disappearance of parent OL and the appearance of OA, AA, and NA products upon ozone exposure is shown in Figure 5. The oleic acid peak (282 amu) decreases steadily from panel *a* to panel *c* in Figure 5 as ozone exposure increases from 0 to 6.6×10^{-5} atm·s. Product peaks for OA (144 amu), AA (152 amu), and NA (158 amu) concomitantly increase, although to observe these results the raw data in Figure 5 must be corrected for remaining oleic acid as by eq 1. NN (142 amu) is not detected, possibly due to its volatility. Moise and Rudich[39] and Thornberry and Abbatt[30] identify NN as a major volatile reaction product.

The loss of parent compound and the appearance of products with increasing ozone exposure are shown in Figure 6. The percent of oleic acid reacted increases steadily with increasing ozone exposure (Figure 6a). We define 95% loss as 1.0 normalized exposure. The normalization is useful for comparison of results among different layer thickness (e.g., Figure 9).

Identification and quantification of the condensed-phase products of the in situ aerosol shows that as OL decreases with increasing ozone exposure, OA, AA, and NA form (Figure 6b,c). The rapid initial formation of the products OA, AA, and NA parallels the loss of the OL parent compound (Figure 6a). The product yields shown in Figure 6c are 35% for OA, 3% for AA, and 1% for NA after 1.0 normalized ozone exposure. Although the run-to-run variability of an individual *m*/*z* value is 5%, we can nevertheless reproducibly observe AA and NA in yields of 1% to 3% by using the information content of the entire mass spectrum in conjunction with the pattern analysis methods implied in eq 1 (i.e., pseudoinverse matrix to obtain the matrix of chemical mass loadings β).

During ozone exposure, the particles evaporate by up to 30% by carbon number as determined by our analysis of the mass spectra. This result is consistent with the decrease in measured particle mobility diameter (Figure 3). If NN is assumed to be the volatile product, then evaporation of 25% by carbon number is expected based upon NN gas-phase product yields reported in the literature.[30,39]

Our results show that AA and NA are minor products. The OA:AA and OA:NA relative yields at 1.0 normalized ozone exposure range from 9 to 18 for the 2 to 30 nm coating thickness studied. This result can be compared to the 1:1 product ratios expected for the gas-phase reactions of ozone with oleic acid.[44]

Our results for the oxidation reaction of condensed-phase oleic acid by ozone can be compared to those reported in the literature (Table 1). Morris et al.[29] do not clearly identify products. Moise and Rudich[39] in an ex situ chromatographic analysis identify AA as a condensed-phase reaction product and NN as a volatile reaction product. Moise and Rudich[39] do not analyze for OA. Smith et al.[33] report a major product, which is tentatively assigned as OA, as well as a small amount of NN. They employ particles several times larger than ours, which may explain why NN does not fully volatilize. Thornberry and Abbatt[30] identify NN as a volatile reaction product. The results of Morris et al.,[29] Moise and Rudich,[39] Smith et al.,[33] and Thornberry and Abbatt[30] are consistent with our observations.

3.3.2. Other $C_xH_yO_z$ Products. After accounting for OL, OA, AA, NN, and NA fragments, a residual mass spectrum remains. Important marker peaks occur at 155, 221, and 265 amu (Figure 7). The intensities of these peaks increase linearly with ozone exposure.

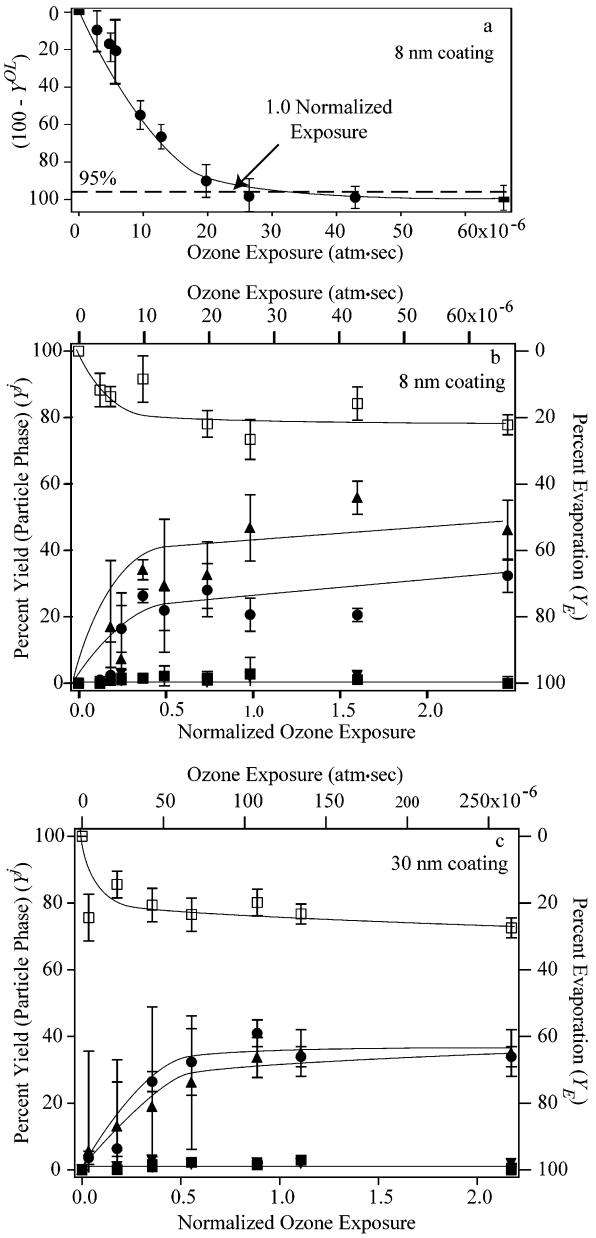

Figure 6. (a) Percent reacted oleic acid ($100 - Y^{OL}$; eq 2) with increasing ozone exposure. We define 95% loss as 1.0 normalized exposure in parts *b* and *c*. The normalization is useful for comparison of results among different layer thickness (e.g., Figure 9). (b) Percent yield (Y^j of eq 2) of condensed-phase products (AA, OA, and CHO_T; left-hand axis) for particles initially having 8 nm OL coatings with increasing ozone exposure. Also shown is the percent change in particle mass (□) (Y_E, right-hand axis), which arises from the evaporation of volatile products. (c) Same as part *b* except for 30 nm coating thickness. Key: (■) AA, (●) OA, (▼) NA, (▲) CHO_T. Lines are drawn in the figures to aid the eye and do not represent a model fit. (The AA and NA data points overlap and are nearly indistinguishable.)

3.3.2.1 Multivariate Analysis. We employ singular value decomposition to explore the variability in the set of mass spectral data from 0 to 2 normalized ozone exposure for 8- to 30-nm coatings. Using 50 mass spectra for pure oleic acid, we establish a variance threshold of 0.89 (i.e., the first singular value divided by the sum of all singular values). The remaining 0.11 variance diagnoses the reproducibility of our experiment. The noise threshold is 0.04, which is the second singular value for pure oleic acid. This result is consistent with our direct observations that the relative intensities making up the fragmentation pattern of oleic acid are reproducible within 5%.

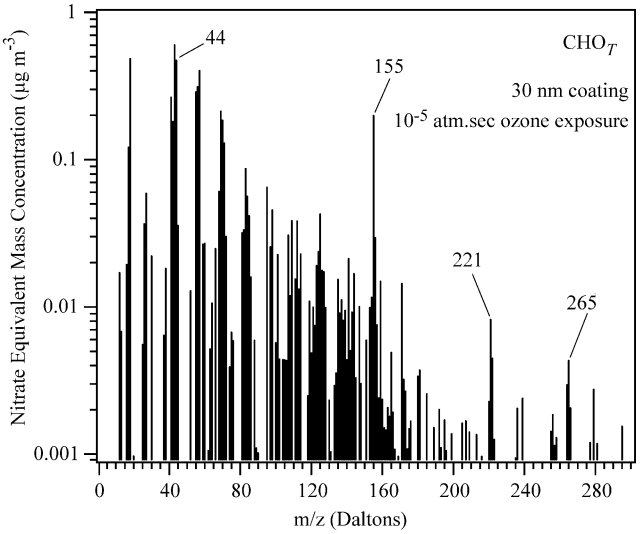

Figure 7. Example of the mass spectrum of the combined products (CHO_T) shown for 30 nm coating and 10^{-5} atm·s ozone exposure. Note that the *y*-axis is log to show the full range of peak intensities.

To establish the minimum number of major components necessary to explain our data in the reacted particles, we select 16 mass spectra for products having normalized ozone exposure greater than 1.0 and 16 mass spectra for unreacted oleic acid. We obtain three singular values above the noise threshold, which we believe correspond to OL, OA, and CHO_T. In addition to these major products, the singular value analysis does not rule out additional minor products below the noise threshold. As discussed below, we believe AA and NA occur as minor products.

To explore the physical basis of the singular value components, we first try to obtain $[\beta]$ by using $[\beta] = [f]^{-1}[m]$ for $[f]$ constituted by the authentic standards OL, OA, AA, and NA. The results show significant contributions by OL and OA; however, the residuals obtained are not satisfactory and there are negative concentrations for AA. We conclude that there must be one or more unidentified chemical species present. When taken together, these species constitute the CHO_T group of molecules.

To isolate the mass spectra of CHO_T, we select *m*/*z* values unique to the known species and assume that the CHO_T products do not contribute significantly at these selected *m*/*z* values. Specifically, we subtract the pure OL standard from all the recorded mass spectra using the 282 peak as the proportionality factor. From these residuals, we then subtract OA using the 144 peak, followed by AA using the 152 peak, followed by NA using the 158 peak. The resulting set of residuals is shown by singular value decomposition to have three singular values above the noise threshold of 0.04. We conclude CHO_T is composed of at least three molecules CHO_a, CHO_b, and CHO_c. Our efforts to deconvolute the CHO_T spectrum (Figure 7) into CHO_a, CHO_b, and CHO_c component spectra yield nonunique results. We believe additional experiments are necessary to better identify CHO_a, CHO_b, and CHO_c.

3.3.2.2. Percent Yield. The uncertainties in the chemical structures of the CHO_T components, especially their oxidation states, provide a challenge for estimating their percent yields. To approach this problem, we assume an OL molecule combines with one of the C_9 radical intermediates. With this assumption, we obtain $n^{CHO_T} = 27$ and $472 < M_W^{CHO_T} < 518$. We can then use eq 2 to calculate percent yield. As shown in eq 2, the ratio $n^{CHO_T}/M_W^{CHO_T}$ is the critical value, rather than our absolute

assumptions of n^{CHO_T} and $M_W^{CHO_T}$. We have $0.62 < 12n^{CHO_T}/M_W^{CHO_T} < 0.68$, which reflects the uncertainty in the oxidation state of the residual organic component. We also assume $RIE^{CHO_T} = 1.4$. The uncertainty bars in Figures 6b,c and 9 reflect this analysis. Panels *b* and *c* in Figure 6 show that as OL decreases with increasing ozone exposure, CHO_T forms as a major product comparable with OA. CHO_T has a higher percent yield for thinner rather than thicker coatings.

3.3.2.3. Proposed Mechanism. Any proposed mechanism is constrained by the following observations:

1. Work by Moise and Rudich[39] and Thornberry and Abbatt[30] shows that the only volatile product formed is NN. Its yield is 25%. Pointedly, CO_2(g) is not observed.

2. We find OA is the major identified condensed-phase product. Its yield is above 25%. The NN yield accounts for 25% yield of OL; the additional OA yield requires that OA be formed by additional pathways.

3. AA and NA form as minor products below 3% yield. The similarities among the chemical structures of OA, AA, and NA indicate similar chemical reactivities in regard to possible further reactions with ozone or Criegee biradicals. To reconcile this similar reactivity with the observations of high OA yield and low AA and NA yields, we infer that AA and NA must never form in great yield. Their precursor species must be scavenged.

4. Additional CHO_T products form at yields above 25%. The mass spectrum of the CHO_T component (Figure 7) shows that these molecules have fragments at high amu values (greater than 200 amu). They therefore contain carbon chains longer than C_9 (i.e., the products of pathways 1 and 2 shown in Figure 1).

The mechanism we propose below is consistent with these four observations.

The formation of CHO_T molecules is hypothesized by us to involve reactions of the Criegee biradical in the condensed phase. The initial products of ozone attack on OL are a Criegee biradical and an aldehyde.[45] In the gas phase, the biradical decomposes into a suite of chemical species, such as RCO, RCOOH, CO_2, CO, H_2O, and OH.[45,46] In solvents, however, the highly energetic Criegee biradical may become stabilized, in which case the decomposition pathways analogous to gas-phase reactions are less important.

For the reaction mechanism in the condensed phase, we propose that ozone adds across the double bond of oleic acid. The molozonide then decomposes by 50:50 channels to form the radical species shown in Figure 8. The key point in our proposed mechanism is that the resulting Criegee biradicals add to the oleic acid double bond as a major pathway to form C_{27} molecules. Rearrangements to AA and NA are minor pathways: this condensed-phase behavior contrasts to gas-phase reactions because the high density of double bonds in condensed-phase oleic acid intercepts the Criegee biradicals before significant AA and NA can form. Cleavage of the five-membered-ring peroxide in the C_{27} molecule can lead to many compounds, including ketones, alkenes, and carboxylic acids (Figure 8). The symmetry of OL leads to the result that the Criegee biradical precursor to AA can instead add to OL, form a peroxide, cleave, and yield OA. As such, the OA yield can exceed 25%, which could explain the OA yields observed in Figure 6. Similarly, the precursor to NA can form C_{27} products (Figure 8), which may be stable or decompose to many possible products, including NN. This NN-formation pathway, however, may not be favorable because there is some evidence against it: gas-phase studies show only a 25% NN yield, which can be fully accounted for by direct decomposition of the primary ozonide (Figure 8).

Although we do not rule out the formation of secondary ozonides by the reaction of the aldehyde products with Criegee biradicals, we do not need to invoke this explanation for our data set. Secondary ozonide formation by the reaction of the Criegee biradical with the C═O groups of NN and OA would be inconsistent with the reported 25% yield of 1-nonanal.[30] This reasoning suggests that Criegee biradicals preferentially react with the double bond of OL despite the initial proximity of the C═O groups of NN and OA in a cage prior to diffusion away from the Criegee biradicals.

The observations also allow several other gas-phase pathways to be ruled out in the condensed phase. A unimolecular decomposition pathway of the Criegee biradical in the gas phase is COO to OCO isomerization followed by release of CO_2, which in the case of OL ozonolysis would lead to the formation of octane instead of NA and octanoic acid instead of AA.[47] In contrast, observations of the gas-phase products show neither octane nor CO_2.[30,39] The absence of this pathway further supports our hypothesized mechanism that the Criegee biradicals react sufficiently rapidly with OL such that the gas-phase reaction pathways are at most minor pathways in the condensed phase.

After 1.0 normalized ozone exposure, the mass spectrum of CHO_T continues to change (not shown). We probe the change at 155 amu for normalized ozone exposure up to 3.0 and observe a continuous increase of the signal. This observation suggests that new reaction pathways open when the supply of OL double bonds is depleted. Possible reactions at this point could include secondary ozonides, although any OA decrease is not detectable within our uncertainty limits (Figure 6). Alternatively, O_3 could react directly with the carboxylic acid groups.[48] Continued direct reactions of CHO_T products with O_3 are thus hypothesized by us as sufficient to continue to process the particles and to alter the mass spectrum of CHO_T. The report by Ziemann[49] of numerous oxygenated organic molecular products including peroxides for the reaction of OL with O_3 is consistent with our observations.

3.3.3. Effect of Layer Thickness. The reacto-diffusive length of ozone in oleic acid is reported as 5,[29] 6,[39] and 20 nm.[33] Hence, varying the coating thickness of oleic acid layers from 2 to 30 nm allows us to probe the transition between reactions that occur mainly in the surface region versus those that occur predominantly in the bulk volume. The overall uptake coefficient γ can be partitioned into contributions from uptake due to reaction at the surface (Γ_{surf}) versus in the bulk (Γ_{bulk}).[33] A future report from us will provide kinetic results (e.g., Figure 6a) for the dependence of γ on layer thickness and hence the partitioning into Γ_{surf} and Γ_{bulk}.

In addition to the different possible rates for the surface versus bulk reaction channels, it is further possible that the relative yield of products is influenced by surface versus bulk chemical environments. As a limiting example to make this point, consider that product A forms only in the bulk chemical environment whereas product B forms only in a surface region of fixed depth. In the case of a 2 nm layer thickness, a 5 nm assumed surface region, and a 10 nm assumed reacto-diffusive length, the yields of product A and B would be 0% and 100%, respectively. Increasing the layer thickness to 10 nm would increase the yield of A and decrease that of B. Increasing the layer thickness beyond 10 nm would continue to produce a mix of A and B, approaching some limiting ratio as determined by the diffusion of oleic acid from the deep interior of particle into the reaction zone (of depth equal to the reacto-diffusive length), which is subdivided into surface and bulk chemical environments. This

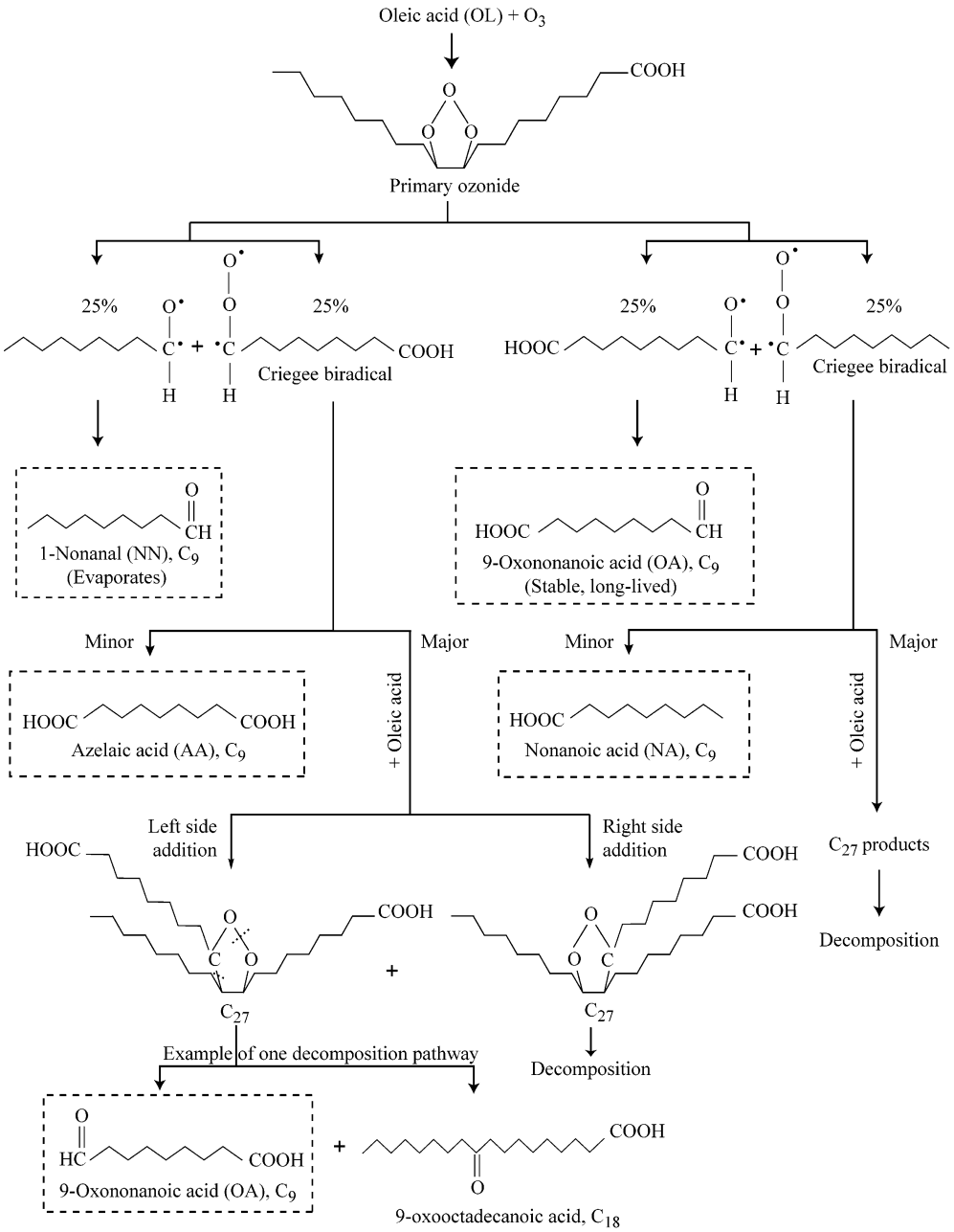

Figure 8. Proposed condensed-phase reaction pathways. The Criegee biradical reacts with oleic acid.

example assumes that the reacto-diffusive length is invariant with regard to the extent of reaction and that the reacto-diffusive length is greater than the depth of the surface region.

The effect of layer thickness on percent yield of condensed-phase products is shown in Figure 9 for 1.0 normalized ozone exposure. CHO_T and OA percent yields appear to decrease and increase respectively with greater layer thickness, suggesting that a surface reaction for CHO_T formation occurs at greater yield than its bulk counterpart and vice versa for OA. Within the uncertainty bars, no trend can be discerned for the AA and NA percent yields for layer thickness varying from 2 to 30 nm.

3.3.4. Particle Oxygen Content. When ozone reacts with oleic acid, there is an increase in the carbon-normalized oxygen content (z/x) in the average chemical composition $C_xH_yO_z$ of the layer. We use the definition

$$(z/x) = \frac{\sum_j (n^j_{O_x}/M_W^j) C^j}{\sum_j (n^j/M_W^j) C^j} \qquad (3)$$

where $n^j_{O_x}$ is the number of oxygen atoms in the molecule j. The numerator of eq 3 is the total moles of oxygen. The denominator of eq 3 is the total moles of carbon. The ratio z/x is anticipated to correlate positively with the hygroscopicity and the density of the overall particle chemistry.

The carbon-normalized oxygen content (z/x) in the average chemical composition $C_xH_yO_z$ of the particle increases with higher ozone exposure (Figure 10). CH_4 has $z/x = 0.0$ while CO_2 has $z/x = 2$. To prepare Figure 10, we employ eq 3 for which limiting assumptions on the molecular structures of CHO_T are necessary. As discussed above for Figure 6b,c, we have $0.62 < 12n^{CHO_T}/M_W^{CHO_T} < 0.68$. We further employ $0.11 < 16n^{CHO_T}_{O_x}/M_W^{CHO_T} < 0.20$ for $3.5 < n^{CHO_T}_{O_x} < 6.5$, which is based on our description that one O_3 molecule adds to oleic acid to yield C_{27} structures via the mechanisms depicted in Figure 8. Namely, these structures have either 4 (NA precursor radical pathway) or 6 (AA precursor radical pathway) oxygen atoms for 27 carbon atoms. An assumption of these structures restricts

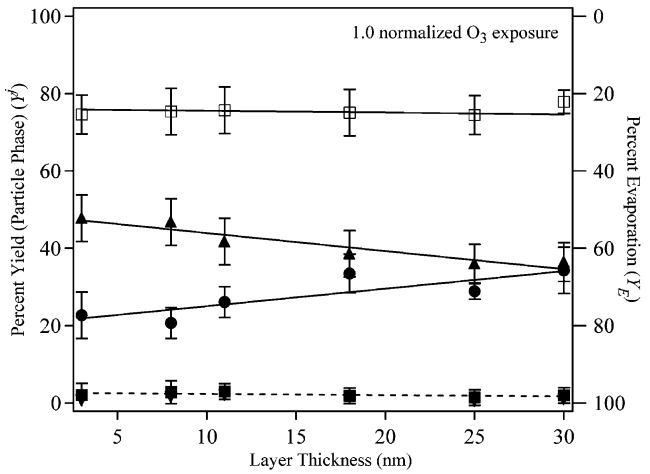

Figure 9. Effect of layer thickness on percent yield (Y^j of eq 2) of condensed-phase products (AA, OA, NA, and CHO_T; left-hand axis) at 1.0 normalized ozone exposure. Also shown is the percent change in particle mass (□) (Y_E, right-hand axis), which arises from the evaporation of volatile products. Key: (■) AA, (●) OA, (▼) NA, (▲) CHO_T. Lines are drawn in the figures to aid the eye and do not represent a model fit. (The AA and NA data points overlap and are nearly indistinguishable.)

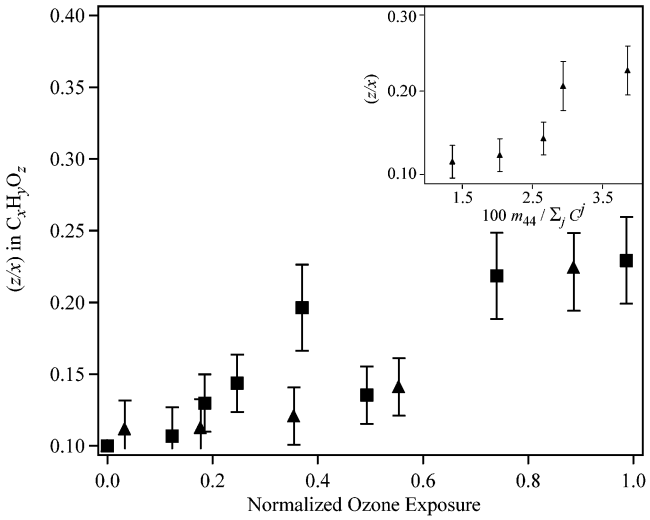

Figure 10. Effect of normalized ozone exposure on carbon-normalized oxygen content (z/x) in the average $C_xH_yO_z$ chemical composition of the layer for 8 (■) and 30 nm (▲) coatings. Shown are the central values with uncertainty estimates showing minimum and maximum values assuming specific limiting molecular structures discussed in the text. Inset: (z/x) versus $100m_{44}/\sum_j C^j$ for 30 nm coating (see text).

the x-axis range of Figure 10 to an upper limit of approximately 1.0 normalized ozone exposure because the calculation assumes only one net O_3 molecule present in the proposed C_{27} structures. Other structures having additional net O_3 content are suggested by the continuous development of the CHO_T mass spectrum for high ozone exposures (section *3.3.2.3*).

Interpretations of AMS measurements of atmospheric particles employ the intensity of the 44-amu peak as an indicator of oxidized organic compounds.[50,51] The intensity is small when sampling primary particles believed to be composed of soot and other materials having small z/x, whereas the intensity increases for aged particles, including secondary organic aerosol. These aged particles are more hygroscopic and have larger z/x. The inset in Figure 10 shows the mass percent of the 44-amu peak in our analyses (given by $100m_{44}/\sum_j C^j$) directly correlates with z/x.

4. Conclusions and Atmospheric Implications

In this paper the reaction products and mechanisms of ozone with multicomponent aerosol particles are studied with oleic acid coated particles as a model system. The results of our study have several atmospheric implications:

1. In our proposed mechanism (Figure 8), condensed-phase ozonolysis leads to radical coupling reactions. Specifically, these products are proposed to form by the reactions of Criegee intermediates with alkenes present in the particles. We speculate that long-chain multifunctional organic molecules result and that these high molecular weight products have low vapor pressures and therefore remain in the condensed phase. Although the formation of high molecular weight compounds such as humic acids[52] has been suggested for reactions of organic molecules in acidic medium,[53] our suggestion of these molecules in the ozonolysis reactions of organic aerosol particles is new.

2. The organic molecules formed by the reactions of oleic acid and ozone are more oxygenated than the parent molecule (i.e., (z/x) increases). The oxygen-enriched organic molecules are expected to have small contact angles with water.[27,34,54] As a result, the reacted particles may act as improved CCN compared to the unreacted hydrophobic particles.[55] The formation of water-soluble molecules such as carboxylic acids may further enhance the hygroscopicity and hence the CCN activity of the reacted particles. The high molecular weight molecules may also be surface active and thus may lower the surface tension of partially activated droplets, thus possibly altering the Köhler curve growth properties of the reacted particles.[14]

3. This study demonstrates that relative product yields depend on whether the reactions occur in the surface or bulk regions of the particle. By extension, we suggest that the reaction products of thin coatings, such as those encapsulating dust particles, may differ from the products formed inside particles having a high fraction of organic matter.

4. This study finds that ozonolysis reactions lead to the formation of volatile products, which are readily released to the gas phase. The ozonolysis reactions studied here lead to 25% mass loss. The particle mass loss is accompanied by unequal changes in the mobility and aerodynamic diameters of the particle, which implies that the density of the reacted particles also changes, apparently due to the addition of oxygen.

The heterogeneous chemistry of organic molecules in atmospheric aerosol particles is complex. Condensed- and gas-phase products and mechanisms differ. Inside the condensed phase, surface and bulk regions have differing chemical reactivities. Our results thus show that the reaction products and mechanisms of organic molecules with ozone may depend not only on the chemical composition of the molecules but also on their physical state and geometrical configuration. Further studies with multicomponent aerosol particles with varying relativity humidity are warranted to further elucidate this complex problem.

Acknowledgment. We are grateful for support received from the National Science Foundation Atmospheric Chemistry Program and the Dreyfus Foundation Postdoctoral Program in Environmental Chemistry.

References and Notes

(1) Seinfeld, J. *National Research Council, Panel on Aerosol Radiative Forcing and Climate Change. A Plan for a Research Program on Aerosol Radiative Forcing and Climate Change*; National Academy Press: Washington, DC, 1996.

(2) Heintzenberg, J. *Chem. Unserer Zeit* **1999**, *33*, 158.

(3) Haywood, J.; Boucher, O. *Rev. Geophys.* **2000**, *38*, 513.

(4) Ramaswamy, V.; Boucher, O.; Haigh, J.; Hauglustaine, D.; Haywood, J. M.; Myhre, G.; Nakajima, T.; Shi, G. Y.; Solomon, S. Radiative Forcing of Climate Change. In *Climate Change 2001*: *The Scientific Basis. Contribution of Working Group I to the Third Assessment Report of the Intergovernmental Panel on Climate Change*; Houghton, J. T., Ding, Y., Griggs, D. J., Noguer, M., Linden, P. v. d., Dai, X., Maskell, K., Eds.; Cambridge University Press: Cambridge, UK, 2001; pp 349ff.

(5) Ramanathan, V.; Crutzen, P. J.; Kiehl, J. T.; Rosenfeld, D. *Science* **2001**, *294*, 2119.

(6) Samet, J. *Research Priorities for Airborne Particular Matter. 1. Immediate Priorities and a Long-Range Research Porfolio*; National Academy Press: Washington, DC, 1998.

(7) Cruz, C. N.; Pandis, S. N. *J. Geophys. Res.* **1998**, *103*, 13111.

(8) Russell, L. M.; Maria, S. F.; Myneni, S. C. B. *Geophys. Res. Lett.* **2002**, *29*, 1029.

(9) Posfai, M.; Xu, H.; Anderson, J. R.; Buseck, P. R. *Geophys. Res. Lett.* **1998**, *25*, 1907.

(10) Falkovich, A. H.; Schkolnik, G.; Ganor, E.; Rudich, Y. *J. Geophys. Res.* **2004**, *109*, D022008.

(11) Tervahattu, H.; Juhanoja, J.; Kupiainen, K. *J. Geophys. Res.* **2002**, *107*, 4319.

(12) Ellison, G. B.; Tuck, A. F.; Vaida, V. *J. Geophys. Res.* **1999**, *104*, 11633.

(13) Saxena, P.; Hildemann, L. M.; McMurry, P. H.; Seinfeld, J. H. *J. Geophys. Res.* **1995**, *100*, 18755.

(14) Facchini, M. C.; Mircea, M.; Fuzzi, S.; Charlson, R. J. *Nature* **1999**, *401*, 257.

(15) Middlebrook, A. M.; Murphy, D. M.; Thomson, D. S. *J. Geophys. Res.* **1998**, *103*, 16475.

(16) Noble, C. A.; Prather, K. A. *Mass Spectrom. Rev.* **2000**, *19*, 248.

(17) Allan, J. D.; Coe, H.; Bower, K. N.; Williams, P. I.; Galanter, M. W.; Alfarra, M. R.; Jimenez, J. L.; Nernitz, E.; McDonald, A. G.; Canagaratna, M. R.; Jayne, J. T.; Worsnop, D. R. *J. Geophys. Res.* **2003**, *108*, 4284.

(18) Novakov, T.; Penner, J. E. *Nature* **1993**, *365*, 823.

(19) Novakov, T.; Corrigan, C. E. *Geophys. Res. Lett.* **1996**, *23*, 2141.

(20) Yu, S. C. *Atmos. Res.* **2000**, *53*, 185.

(21) Jacobson, M. C.; Hansson, H. C.; Noone, K. J.; Charlson, R. J. *Rev. Geophys.* **2000**, *38*, 267.

(22) Charlson, R. J.; Seinfeld, J. H.; Nenes, A.; Kulmala, M.; Laaksonen, A.; Facchini, M. C. *Science* **2001**, *292*, 2025.

(23) Seinfeld, J. H.; Pandis, S. N. *Atmospheric Chemistry & Physics*: *From Air Pollution to Climate Change*; Wiley: New York, 1998.

(24) Andreae, M. O. *Nature* **2001**, *409*, 671.

(25) Andreae, M. O.; Crutzen, P. J. *Science* **1997**, *276*, 1052.

(26) Rudich, Y. *Chem. Rev.* **2003**, *103*, 5097.

(27) Moise, T.; Rudich, Y. *J. Geophys. Res.* **2000**, *105*, 14667.

(28) Moise, T.; Talukdar, R. K.; Frost, G. J.; Fox, R. W.; Rudich, Y. *J. Geophys. Res.* **2002**, *107*, 1029.

(29) Morris, J. W.; Davidovits, P.; Jayne, J. T.; Jiménez, J. L.; Shi, Q.; Kolb, C. E.; Worsnop, D. R.; Barney, W. S.; Cass, G. *Geophys. Res. Lett.* **2002**, *29*, 9.

(30) Thornberry, T.; Abbatt, J. P. D. *Phys. Chem. Chem. Phys.* **2004**, *6*, 84.

(31) Tobias, H. J.; Ziemann, P. J. *Anal. Chem.* **1999**, *71*, 3428.

(32) Grassian, V. H. *Int. Rev. Phys. Chem.* **2001**, *20*, 467.

(33) Smith, G. D.; Woods, I. E.; DeForest, C. L.; Baer, T.; Miller, R. E. *J. Phys. Chem. A* **2003**, *106*, 8085.

(34) Bertram, A. K.; Ivanov, A. V.; Hunter, M.; Molina, L. T.; Molina, M. J. *J. Phys. Chem. A* **2001**, *105*, 9415.

(35) Mulholland, G. W.; Bryner, N. P.; Croarkin, C. *Aerosol Sci. Technol.* **1999**, *55*, 31.

(36) Wadia, Y.; Tobias, D. J.; Stafford, R.; Finlayson-Pitts, B. J. *Langmuir* **2000**, *16*, 9321.

(37) Weingartner, E.; Burtscher, H.; Baltensperger, U. *Atmos. Environ.* **1997**, *31*, 2311.

(38) Rogge, W. F.; Hildemann, L. M.; Mazurek, M. A.; Cass, G. R.; Simonelt, B. R. T. *Environ. Sci. Technol.* **1991**, *25*, 1112.

(39) Moise, T.; Rudich, Y. *J. Phys. Chem. A* **2002**, *106*, 6469.

(40) Han, J. H.; Martin, S. T. *Aerosol Sci. Technol.* **2001**, *34*, 363.

(41) Broekhuizen, K. E.; Kumar, P. P.; Abbatt, J. P. D. American Geophysical Union Fall Meeting, San Francisco, 2003.

(42) Jayne, J. T.; Leard, D. C.; Zhang, X.; Davidovits, P.; Smith, K. A.; Kolb, C. E.; Worsnop, D. R. *Aerosol. Sci. Technol.* **2000**, *33*, 49.

(43) NIST Chemistry Webbook; http://Webbook.Nist.Gov/Chemistry/, 2003.

(44) Atkinson, R.; Carter, W. P. L. *Chem. Rev.* **1984**, *84*, 437.

(45) Criegee, R. *Angew. Chem., Int. Ed. Engl.* **1975**, *14*, 745.

(46) Finlayson-Pitts, B. J.; Hemminger, J. C. *J. Phys. Chem. A* **2000**, *104*, 11463.

(47) Eliason, T. L.; Aloisio, S.; Donaldson, D. J.; Cziczo, D. J.; Vaida, V. *Atmos. Environ.* **2003**, *37*, 2207.

(48) Nepotchatykh, O. V.; Ariya, P. A. *Environ. Sci. Technol.* **2002**, *36*, 3265.

(49) Ziemann, P. J. American Association for Aerosol Research Annual Meeting, Anaheim, 2003.

(50) Allan, J. D.; Jimenez, J. L.; Williams, P. I.; Alfarra, M. R.; Bower, K. N.; Jayne, J. T.; Coe, H.; Worsnop, D. R. *J. Geophys. Res.* **2003**, *108*, 4283.

(51) Allan, J. D.; Alfarra, M. R.; Bower, K. N.; Williams, P. I.; Gallagher, M. W.; Jimenez, J. L.; McDonald, A. G.; Nemitz, E.; Canagaratna, M. R.; Jayne, J. T.; Coe, H.; Worsnop, D. R. *J. Geophys. Res.* **2003**, *108*, 4284.

(52) Gelencser, A.; Hoffer, A.; Kiss, G.; Tombacz, E.; Kurdi, R.; Bencze, L. *J. Atmos. Chem.* **2003**, *45*, 25.

(53) Duncan, J. L.; Schindler, L. R.; Roberts, J. T. *J. Phys. Chem. B* **1999**, *103*, 7247.

(54) Moise, T.; Rudich, Y. *Geophys. Res. Lett.* **2001**, *28*, 4083.

(55) Raymond, T. M.; Pandis, S. N. *J. Geophys. Res.* **2002**, *107*, 4787.